Computers and Concrete, *Vol. 22, No. 6 (2018) 551-561*
DOI: https://doi.org/10.12989/cac.2018.22.6.551

A study on ITZ percolation threshold in mortar with ellipsoidal aggregate particles

Zichao Pan*, Dalei Wang[a], Rujin Ma[a] and Airong Chen[b]

Department of Bridge Engineering, Tongji University, 1239 Siping Road, Shanghai, 200092, China

(Received October 10, 2018, Revised November 29, 2018, Accepted November 30, 2018)

Abstract. The percolation of interfacial transition zone (ITZ) in cementitious materials is of great importance to the transport properties and durability issues. This paper presents numerical simulation research on the ITZ percolation threshold of mortar specimens at meso-scale. To simulate the meso-scale model of mortar as realistically as possible, the aggregates are simplified as ellipsoids with arbitrary orientations. Major and minor aspect ratios are defined to represent the global shape characteristics of aggregates. Some algorithms such as the burning algorithm, Dijkstra's algorithm and Connected-Component Labeling (CCL) algorithm are adopted for identification of connected ITZ clusters and percolation detection. The effects of gradation and aspect ratios of aggregates on ITZ percolation threshold are quantitatively studied. The results show that (1) the ITZ percolation threshold is mainly affected by the specific surface area (SSA) of aggregates and shows a global decreasing tendency with an increasing SSA; (2) elongated ellipsoidal particles can effectively bridge isolated ITZ clusters and thus lower the ITZ percolation threshold; (3) as ITZ volume fraction increases, the bridging effect of elongated particles will be less significant, and has only a minor effect on ITZ percolation threshold; (4) it is the ITZ connectivity that is essentially responsible for ITZ percolation threshold, while other factors such as SSA and ITZ volume fraction are only the superficial reasons.

Keywords: interfacial transition zone; mortar; percolation threshold; ellipsoid; gradation

1. Introduction

It is well known that the microstructure of the cement paste near aggregate surface is highly different from that of the bulk cement paste. This special microstructure in the vicinity of an aggregate, termed as "interfacial transition zone" (ITZ), has been comprehensively studied since 1990s (Delagrave *et al.* 1997, Liao *et al.* 2004, Lutz *et al.* 1997, Ollivier *et al.* 1995, Prokopski and Halbiniak 2000, Scrivener and Nemati 1996, Shane *et al.* 2000). The formation of ITZ is mainly due to the "wall effect" caused by aggregates on the packing of cement particles. Usually, the size of the aggregate, even the fine aggregate (0.15~4.75 mm), is much larger than that of the cement particle (<0.1 mm). Thus, during the packing procedure, the aggregate surface is a "wall", which can result in a smaller content of cement particles near the aggregate surface. Thus, after the cement particles are hydrated, different microstructures are formed in the cement paste and eventually result in the formation of ITZ. According to some published experimental researches, the ITZ has a much higher porosity than the bulk cement paste, which implies the significance of ITZ in the transport properties (Yang and Su 2002, Yang *et al.* 2015) and mechanical behavior (Lee and Park 2008) of cementitious materials.

*Corresponding author, Assistant Professor
E-mail: z.pan@tongji.edu.cn
[a]Associate Professor
[b]Professor

Since the ITZ is mainly formed due to the "wall effect" of aggregates on cement particles, the ITZ thickness is determined by the size of cement particles and is irrelevant to the size of aggregates. Experimental observations (Ollivier *et al.* 1995, Scrivener and Nemati 1996) showed that the typical ITZ thickness is usually 10~50 μm, dependent on the fineness of cement particles and mineral admixtures such as fly ash, silica ash, etc. Thus, in numerical modelling, the ITZ is usually considered as a soft shell with an identical thickness surrounding the aggregate. Different from aggregates as solid particles which are not permitted to be overlapped with one another, the individual ITZs can be interconnected to form a cluster, which can eventually develop through the entire specimen, which is usually called the "percolation effect". The percolation of the specimen will greatly facilitate the ingress of external harmful agents such as chloride ions and carbon dioxide, since a connected path with a high porosity is formed through the entire specimen. It is apparent that whether the specimen can be percolated is strongly dependent on the ITZ volume fraction. With a small aggregate volume fraction, the individual ITZs are almost isolated. As more and more aggregates are used, the individual ITZs will be gradually interconnected together and eventually percolate the entire specimen. Thus, there exists a threshold of aggregate volume fraction (termed as "ITZ percolation threshold") above which the specimen can be percolated, while below which the individual ITZs may be partially interconnected but no path across the entire specimen is formed.

Up to now, numerous theoretical and experimental researches have been conducted to find the above ITZ

ISSN: 1598-8198 (Print), 1598-818X (Online)

percolation threshold. Especially, most of theoretical researches used the computer simulation method with the "hard-core/soft-shell" model, where the aggregate is modelled as a "hard" sphere (Winslow *et al.* 1994, Zheng and Zhou 2007) or ellipsoid (Bentz *et al.* 1994) which is not allowed to be overlapped, while the ITZ is taken as a "soft" shell which is permitted to be interconnected. In studying the porosity of a mortar specimen with different volume fractions of sand by the Mercury Intrusion Porosimetry (MIP), Winslow *et al.* (1994) found that the ITZ percolation threshold is in the range of 0.448~0.486. By modelling the aggregate as an ellipsoidal particle, Bentz *et al.* (1994) found that as the aspect ratio increases (aggregate becomes more elongated), significantly lower aggregate contents are needed to form a percolated path through the microstructure. In studying the high-performance concrete (HPC) with fibers, Bentz (2000) found that HPC has a thinner ITZ and lower probability of percolation, but the presence of fibers in the concrete can provide alternative path to percolate the specimen. Zheng and Zhou (2007) studied the effect of aggregate gradation on ITZ percolation threshold. It was found that the Fuller's gradation can result in a larger ITZ percolation threshold than the gradation of Equal Volume Fraction (EVF). Compared with the spherical and ellipsoidal aggregate models, more advanced aggregate models (Qian 2012) were adopted in recent researches (Rypl and Bým 2012), but no related results have been reported yet. The reason is that to obtain the accurate ITZ percolation threshold by the computer simulation method, hundreds or even thousands of simulations are needed to eliminate the effect of randomness from the meso-scale model on a single simulated result. Thus, if the aggregate model is over-complex, the amount of the computational work will be unacceptable in a statistical analysis.

Compared with theoretical researches, the experimental work was greatly insufficient. Most of the theoretical researches used the results of the MIP test by Winslow *et al.* (1994) to validate the models. But Diamond (2003) expressed a different opinion. Based on the backscatter SEM investigations of "duplicate" and original mortar specimens, Diamond (2003) concluded that the MIP test data obtained by Winslow *et al.* (1994) cannot be used to validate the common "hard-core/soft-shell" model, as the sharp increase of the porosity observed in MIP test may be attributed to the interconnected highly porous hardened cement paste (HCP) patches, instead of the geometric overlap of the ITZs. The findings of Diamond (2003) were based on the concept of two distinct HCP patches, i.e., porous patch and dense patch, which can be observed in the backscatter SEM. However, as pointed out by Wong and Buenfel (2006), the HCP patches are artefact of sample preparation and does not reflect the true nature of the hydrated cement paste. But the research by Wong and Buenfel (2006) did not bring additional supports to the classic "hard-core/soft-shell" model. Some other researches on the topic of percolation can be also found in (Wu *et al.* 2015, Ye 2005). But these researches mainly focused on the effect of percolated ITZs on properties of cementitious materials or the percolation of capillary pores at micro-scale and thus did not explicitly give any percolation threshold in terms of the aggregate volume fraction.

To compare with the result of MIP test, early researches (Bentz 2000, Bentz *et al.* 1994, Winslow *et al.* 1994) used the connected ITZ volume fraction to represent the percolation condition of a meso-scale model. This approach can only give an estimated range, instead of an exact value of ITZ percolation threshold. According to the method commonly used in theoretical physics (Rintoul and Torquato 1997), percolation probability as a function of particle volume fraction is needed to determine the percolation threshold. Thus, in a more recent publication (Zheng and Zhou 2007), percolation probability was chosen as the main concern to evaluate the exact percolation threshold. But the aggregate in (Zheng and Zhou 2007) was just simplified as a sphere and only two special gradations, i.e., the Fuller's and EVF gradations, were investigated. The effects of aggregate characteristics such as gradation and shape on ITZ percolation threshold were attributed to the specific surface area (SSA) and surface-to-surface distance (SSD) in (Bentz *et al.* 1994) and (Zheng and Zhou 2007), respectively.

By following the philosophy of previous researches, this paper provides a further investigation on ITZ percolation threshold of a meso-scale model with ellipsoidal aggregate particles for cementitious materials. The main contribution of this paper lies in two aspects. Firstly, the exact ITZ percolation threshold, instead of approximate ranges, for different possible gradations and aspect ratios of aggregates are given. Secondly, we will show that SSA is not the single reason responsible for ITZ percolation threshold. The "bridging effect" caused by elongated ellipsoidal aggregates is also one of the reasons. To decrease the computational work and speed up the simulation, the numerical analysis in this paper is only conducted at the scale of mortar, which means that the aggregate size in the meso-scale model is in the range of 0.015~4.75 mm. But the qualitative conclusions can be extended up to the scale of concrete, as the meso-scale models of mortar and concrete are essentially the same in mathematics.

2. Models and methods

2.1 Meso-scale model

2.1.1 Gradation

According to the specifications in Chinese code (GB/T 14684-2011) for sand used in civil engineering, the permitted upper and lower bounds of gradations for coarse, medium and fine natural sand are plotted in Fig. 1. Based on these specifications, six gradations shown in Table 1 are chosen in this paper to study the effect of aggregate gradation on ITZ percolation threshold. The fineness module (FM) for each gradation can be calculated by

$$\mathrm{FM} = \frac{(A_2 + A_3 + A_4 + A_5 + A_6) - 5A_1}{100 - A_1} \tag{1}$$

where A_1, A_2, A_3, A_4, A_5, A_6 are cumulative percentages of aggregate retained on sieves of 4.75 mm, 2.36 mm, 1.18 mm, 0.6 mm, 0.3 mm and 0.15 mm,

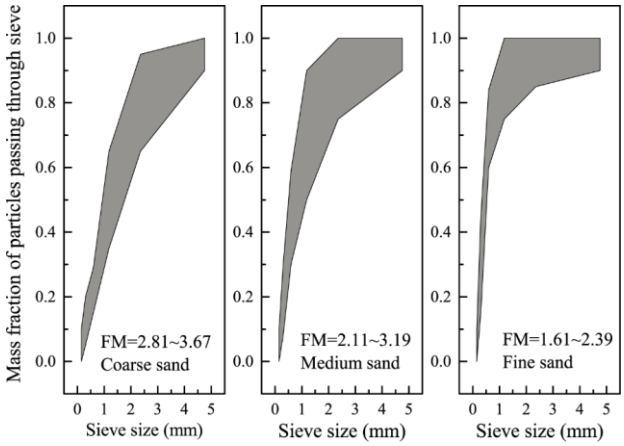

Fig. 1 Gradations of coarse, medium and fine natural sands in Chinese code (GB/T 14684-2011)

Table 1 Aggregate gradations used in numerical analysis in this paper

Sieve size (mm)	I	II	III	IV	V	VI	Exp.
0.15	0.00	0.00	0.00	0.00	0.00	0.00	0.00
0.30	0.45	0.30	0.15	0.20	0.08	0.05	0.21
0.60	0.84	0.59	0.60	0.29	0.30	0.15	0.41
1.18	1.00	0.90	0.75	0.65	0.50	0.35	0.65
2.36		1.00	0.85	0.95	0.75	0.65	0.94
4.75			1.00	1.00	1.00	1.00	1.00

respectively. According to Eq. (1), FMs for the selected six gradations in Table 1 are in the range of 1.71~3.80.

2.1.2 Ellipsoidal particles

In numerical simulation researches on cementitious materials at meso-scale, aggregates have been modelled as two-dimensional circle (Bazant *et al.* 1990), ellipse (Pan *et al.* 2014) and polygon (Pan *et al.* 2015) or three-dimensional sphere (Šavija *et al.* 2013), ellipsoid (Leite *et al.* 2004) and other more complex geometries (Hafner *et al.* 2006, Qian 2012). In this paper, the aggregate shape is simplified as an ellipsoidal particle with arbitrary orientations. This simplification is especially reasonable for sand and pebbles.

In 3D Euclidean space, an ellipsoid can be uniquely defined by nine parameters, i.e., $a, b, c, x_c, y_c, z_c, \alpha, \beta, \gamma$, where a, b, c $(a \geq b \geq c)$ are the lengths of three semi axes, (x_c, y_c, z_c) are the Cartesian coordinates of the center and α, β, γ are the orientations of the ellipsoid. To describe the aggregate shape, major and minor aspect ratios are defined as $\xi_1 = a/b$ and $\xi_2 = b/c$, respectively. The procedure to use ellipsoidal particles to construct the meso-scale model of mortar can be divided into two separated parts, i.e., particle shape and packing. With a given arbitrary gradation $P_i(D_i), i = 1,2 \ldots n$, where $P_i(D_i)$ is the passing percentage of aggregates through the sieve with the size of D_i, the sizes of all ellipsoidal particles in a Representative Volume Element (RVE) with the size L can be determined as follows.

1. Set $i = n - 1$.
2. Set $V_i = 0$.
3. Generate a pseudo-random number w on the interval [0,1].
4. A reference sphere with radius $r = w(D_{i+1} - D_i) + D_i$ is generated.
5. The size of the ellipsoidal particle corresponding to the reference sphere is $c = r/\sqrt[3]{\xi_1 \xi_2^2}$, $b = \xi_2 c$ and $a = \xi_1 b$ by assuming that the particle volume is unchanged.
6. Calculate the particle volume as $V = 4\pi abc/3$, and record the particle into computer memory.
7. Add V to V_i, i.e., $V_i = V_i + V$, and check whether $V_i > L^3 f_a (P_{i+1} - P_i)$, where f_a is the required aggregate volume fraction. If not, go to Step 3.
8. Calculate $\varepsilon = \frac{V_i - L^3 f_a (P_{i+1} - P_i)}{L^3 f_a (P_{i+1} - P_i)}$, and check whether $\varepsilon < \varepsilon_0$, where ε_0 is a pre-defined permitted error ($\varepsilon_0 = 0.001$ is used in this paper). If not, go to Step 2.
9. Let $i = i - 1$, and go to Step 2

The whole procedure stops when $i = 0$. In the above procedure, Step 8 is important and cannot be neglected. Otherwise, the gradation of simulated aggregates may be different from what is required, especially in a small RVE with a small aggregate volume fraction due to incorrect size of the last particle in each division ($[D_i, D_{i+1}]$) of the gradation. When the sizes of all aggregates are determined, the orientations are simply randomly generated on the interval $[0,2\pi]$.

The procedure to distribute particles follows a classic "take-and-place" algorithm (Wang *et al.* 1999). During the procedure, a separation check is needed to ensure that the "to-be-placed" particle is not overlapped with any particle which is already in the model. In this paper, the algorithm proposed by Wang *et al.* (2001) is used to conduct the separation check for ellipsoidal particles. The advantage of the closed-form algorithm is the accuracy and efficiency: only the signs rather than the exact values of the roots of a quartic polynomial equation are needed to be evaluated. A detailed implementation of the separation check based on the above algorithm can be found in (King 2008). To eliminate the "wall effect" from the boundary of REV on the particle packing, the periodic boundary condition is applied on every face of RVE. During the packing procedure, more and more separation checks must be conducted to determine the proper position of one particle, which will greatly decrease the simulation efficiency. To speed up the packing procedure, RVE is divided into several sub-RVEs. When the position of a particle is determined, it is assigned to the sub-REVs which completely contains or partially intersected by the particle. When a new particle is to be placed, the sub-REVs which the new particle belongs to are firstly identified based on its potential position. Then, only the separation checks between the new particle and particles which belong to the same sub-REVs are conducted. In this approach, the number of separation checks can be greatly decreased, and the packing procedure can be accelerated as a result. Fig. 2 shows a typical example of simulated meso-scale model with ellipsoidal particles.

2.1.3 Aspect ratio of aggregates

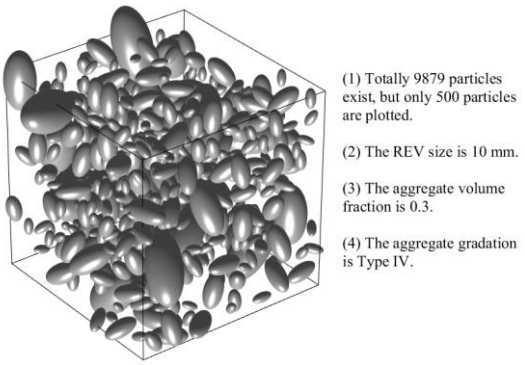

Fig. 2 An example of meso-scale model using ellipsoidal particles with periodic boundary condition

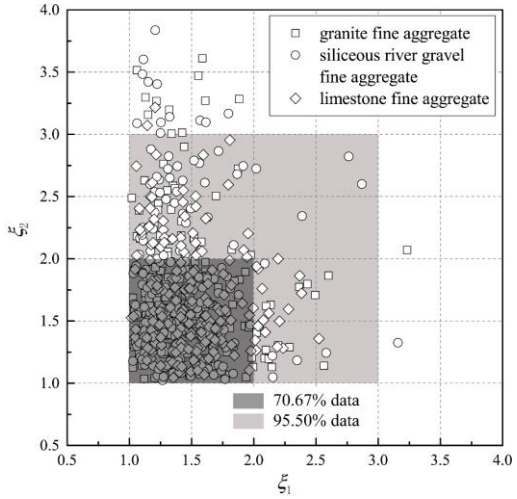

Fig. 3 Distributions of major and minor aspect ratios of fine aggregates based on test data in (Erdogan 2005)

The aspect ratio is the most important parameter to represent the global characteristic of aggregate shape. It describes the degrees of elongation and flatness of an aggregate. The aspect ratio of an aggregate is usually determined based on its corresponding bounding box which can be obtained by an image processing method. For example, by using X-ray tomographic method, Erdogan (2005) calibrated several geometrical parameters including three principal dimensions of an aggregate, i.e., longest dimension (L), intermediate dimension (W) and shortest dimension (T), which can be considered as the length, width and height of the bounding box of an aggregate. Based on the definition of aspect ratio in this paper, the major and minor aspect ratios of one aggregate can be calculated as $\xi_1 = L/W$ and $\xi_2 = W/T$, respectively. Fig. 3 shows the distribution of (ξ_1, ξ_2) based on the measured data of fine aggregates in (Erdogan 2005). It is found that $\xi_1(\xi_2) = 1.0\sim2.0$ and $\xi_1(\xi_2) = 1.0\sim3.0$ can cover 70.67% and 95.50% of the data, respectively. Thus, only the aspect ratios in the range of 1.0~3.0 will be investigated in this paper.

2.1.4 Aspect ratio of aggregates

In this paper, the SSA for a meso-scale model with ellipsoidal particles is defined as

$$\mathrm{SSA} = \frac{\sum_{i=0}^{N} S_i}{\sum_{i=0}^{N} V_i} \tag{2}$$

where S_i and V_i are the surface area and volume of the ith ellipsoidal particle, respectively. The surface area of an ellipsoid is calculated by the Thomsen's formula

$$S \approx 4\pi \sqrt[p]{\frac{a^p b^p + a^p c^p + b^p c^p}{3}} \tag{3}$$

where $p = 1.6075$. Based on Eq. (3), SSA in (2) can be finally calculated by

$$\mathrm{SSA} = f(\xi_1, \xi_2) \frac{\sum_{i=0}^{N} r_i^2}{\sum_{i=0}^{N} r_i^3} \tag{4}$$

where r_i is the radius of reference sphere corresponding to the ith ellipsoidal particle while $f(\xi_1, \xi_2)$ is

$$f(\xi_1, \xi_2) = \frac{\sqrt[p]{3^{p-1}(\xi_1^p \xi_2^{2p} + \xi_1^p \xi_2^p + \xi_2^p)}}{\sqrt[3]{\xi_1^2 \xi_2^4}} \tag{5}$$

Thus, SSA is only dependent on gradation and aspect ratios of aggregates, and irrelevant to RVE size and aggregate volume fraction.

2.1.5 Aspect ratio of aggregates

As soft shells, the ITZs in meso-scale model can be overlapped. Thus, the ITZ volume fraction should be determined in a numerical approach as follows. After aggregate packing procedure is finished, totally N_p points are randomly placed into REV. The number of points (denoted as n_p) which are located inside ITZs are counted. Then, the probability that a random point is located inside ITZs is $n_\mathrm{p}/N_\mathrm{p}$. Based on the Monte-Carlo method, this probability equals to the ITZ volume fraction

$$f_\mathrm{ITZ} = \frac{n_\mathrm{p}}{N_\mathrm{p}} \tag{6}$$

To ensure the accuracy of calculated ITZ volume fraction, $N_\mathrm{p} = 1000000$ is used throughout this paper.

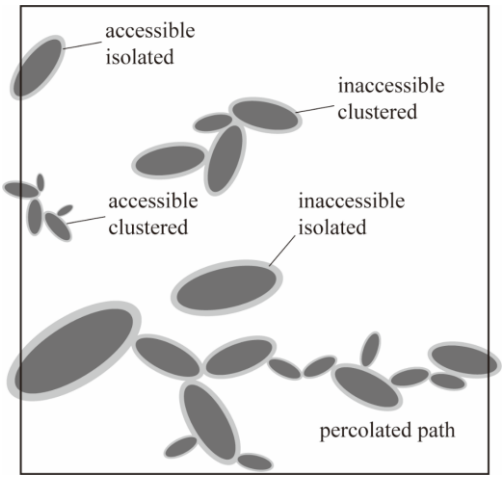

Fig. 4 A schematic of different states of ITZs inside meso-scale model

2.2 Meso-scale model

2.2.1 Accessible ITZ and cluster

The ITZs in the meso-scale model can be categorized into several kinds, as shown in Fig. 4. Based on "burning algorithm" in *x*, *y* and *z* directions, the accessible ITZs can be identified by the following pseudo-codes, where sets *D* and *C* contains all the accessible and inaccessible ITZs, respectively. The RVE sample used here is placed so that its corner coincides with the origin.

```
for each particle i in REV
   if (ITZ of particle i is intersected by surface x=0) then
      Put particle i into set B
   else
      Put particle i into set C
   end if
end for
do while ((set C is not empty) and (set C is changed))
   for each particle i in B
      for each particle j in C
      if (ITZs of particles i and j are overlapped) then
         Put particle j into set B
         Remove particle j from set C
      end if
   end for
   Put particle i into set D
   Remove particle i from set B
   end for
end while
```

If any accessible ITZ is intersected by the surface $x = L$ of REV, the REV is considered as percolated. Based on the identified accessible ITZs, the shortest percolated pathway (shortest distance between central positions of ellipsoids in percolated network) can be found by the Dijkstra's algorithm (Dijkstra 1959). A typical example is shown in Fig. 5. Different clusters can be also identified by the Connected-Component Labeling (CCL) method (Samet and Tamminen 1988), as illustratively shown in Fig. 6. Based on the largest ITZ cluster by volume in REV, the following parameter called "ITZ connectivity" can be defined

$$\phi = \frac{f_{\mathrm{cITZ}}}{f_{\mathrm{ITZ}}} \tag{7}$$

where f_{cITZ} is the volume fraction of ITZs belonging to the largest cluster. Obviously, this parameter represents to what degree ITZs are interconnected. Thus, a larger ϕ usually stands for a higher percolation probability and vice versa.

2.2.2 ITZ Percolation probability

Each simulated meso-scale model can be either percolated or not. Thus, by doing N simulations, the ITZ percolation probability can be simply calculated by

$$p = \frac{n}{N} \tag{8}$$

where n is the number of simulations where REVs are percolated. Obviously, Eq. (8) is only valid when N is large enough, and the accuracy of calculated percolation probability increases with N. But a large N will dramatically increase the computational work at the same time.

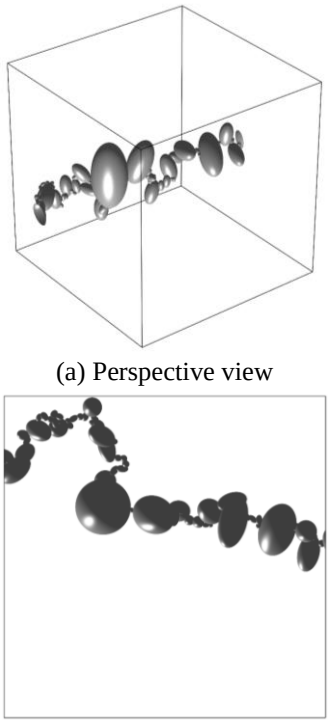

(a) Perspective view

(b) Top view

Fig. 5 An example of identified shortest percolated pathway through REV by Dijkstra's algorithm

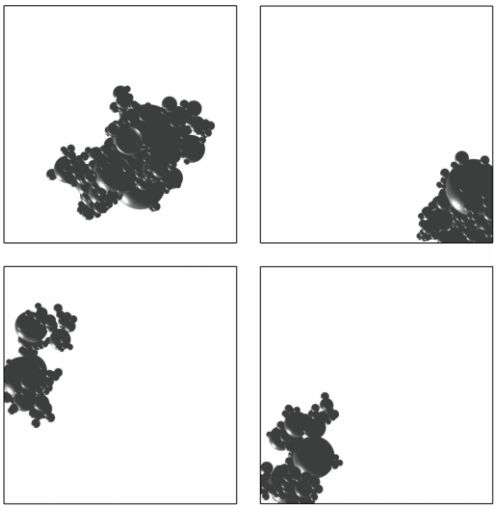

Fig. 6 An example of four largest identified clusters in REV by CCL

The minimum required N for a satisfying accuracy of ITZ percolation probability is related to the parameters such as REV size and characteristics of aggregates. To avoid an over-complex analysis, the same N is used in different cases throughout this paper as an approximation. N is determined by a typical case study where $L = 10\mathrm{mm}$, $\xi_1 = \xi_2 = 2.0$, $f_{\mathrm{a}} = 0.3$, $t_{\mathrm{ITZ}} = 30\,\mu\mathrm{m}$ and Type IV gradation (see Fig. 1). The results of ITZ percolation probability with different N in this case study are shown in Fig. 7. The error in the figure is defined as

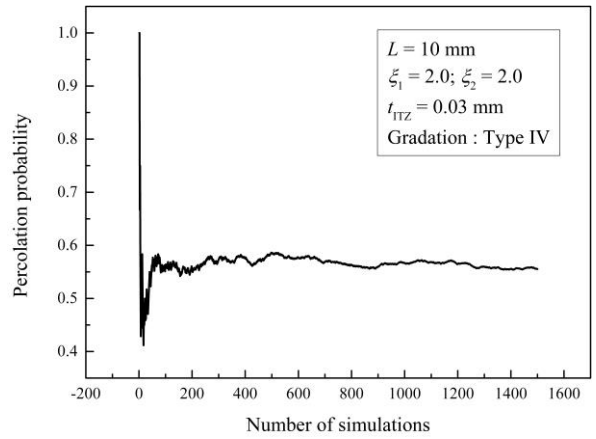

(a) Percolation probability

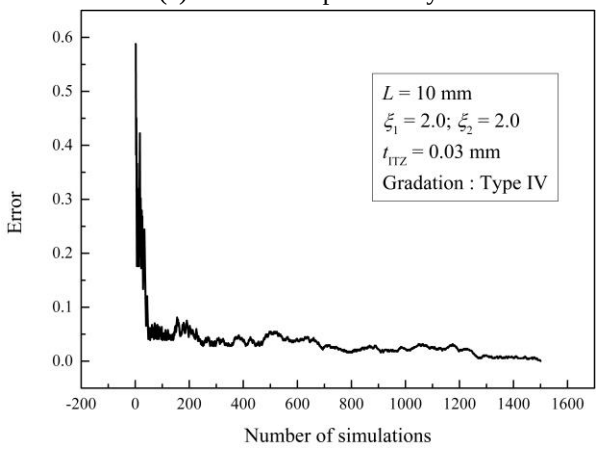

(b) Error

Fig. 7 Effect of N on accuracy of simulated percolation probability

$$\varepsilon(N) = \max\left\{\frac{|p(i) - p(N)|}{p(N)}\right\} \quad i = N+1, N+2, \ldots \quad (9)$$

Based on the results in Fig. 7, it is found that when $N = 1000$, the error ε is as small as 0.023, which means that the percolation probability will not obviously change even if more simulations are conducted. Thus, $N = 1000$ is used throughout this paper. With different aggregate volume fractions used in simulation, the percolation probability can be finally expressed as a function of aggregate volume fraction, i.e., $p = p(f_a)$, which is needed to determine ITZ percolation threshold.

2.2.3 ITZ Percolation threshold

When the ITZ percolation probability as a function of aggregate volume fraction is obtained, the ITZ percolation threshold is determined by fitting the data of percolation probability with the following equation (Rintoul and Torquato 1997)

$$p = 0.5\{1 + \tanh[(f_a - f_c)/\lambda]\} \quad (10)$$

where f_c is the ITZ percolation threshold and λ is the width of percolation transition. A smaller λ stands for a sharper increase of percolation probability at the threshold. Several fitting results are shown in Fig. 8 as an illustration.

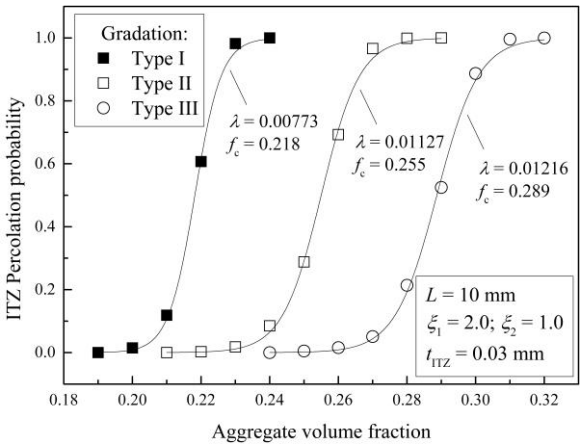

Fig. 8 Examples of data fitting with percolation probability to obtain ITZ percolation threshold

3. Model validation

3.1 Meso-scale model

The computer program to construct the meso-scale model is validated by two approaches. In the first approach, the aggregate volume fraction in the meso-scale model is determined by the similar numerical method to calculate the ITZ volume fraction in Section 2.1.5. If the calculated aggregate volume fraction is much smaller than the requested one, it means that some aggregates are overlapped with one another, which indicates the incorrectness of separation check in developed computer program. In the other approach, the spacing between any two ellipsoidal particles is calculated based on their closest distance which can be numerically solved by the method in (Zheng *et al.* 2009, Zheng and Palffy-Muhoray 2007). In a normal meso-scale model with no overlaps between particles, all ellipsoidal particle spacings should be positive.

3.2 Percolation detection

3.2.1 Theoretical physics

In theoretical physics, a lot of researches have been conducted to obtain the percolation threshold of a system containing particles with a typical shape, i.e., circle (Quintanilla and Ziff 2007), ellipse (Li *et al.* 2016, Xia and Thorpe 1988), rectangle (Li 2013), sphere (Rintoul and Torquato 1997), ellipsoid (Garboczi *et al.* 1995). But different from the model in this paper, the particles in these researches can be overlapped with one another, and no ITZ is concerned. Thus, these models can be described as "soft-core/no-shell" models. To use the results in these theoretical researches, the codes for separation check during particle packing procedure are excluded from the computer program, and the ITZ thickness is set as zero.

Fig. 9 plots several comparisons between theoretical results from (Garboczi *et al.* 1995) and simulation results obtained in this paper. As can be seen, the simulation result has a satisfying agreement with theoretical results, which can validate the correctness of percolation detection in the computer program developed in this research.

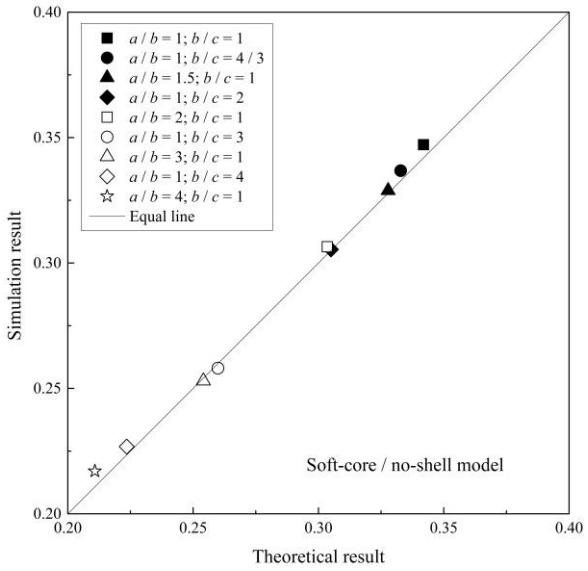

Fig. 9 Comparisons between theoretical and simulation results of percolation thresholds in soft-core/no-shell system with ellipsoidal particles

3.2.2 MIP test

Besides the above comparisons with theoretical researches in physics, the experiment data from (Winslow *et al.* 1994) is also adopted to verify the developed computer program for percolation detection. In the experimental research, Winslow *et al.* (1994) conducted MIP tests on a series of mortar specimens with different volume fractions of sand. It was found that when the volume fraction changes from 0.448 to 0.486, a sharp increase in the porosity was observed in MIP test. The reason for this phenomenon was attributed to the percolation effect by Winslow *et al.* (1994). However, different opinions have been proposed afterwards, as reviewed in Introduction of this paper. According to the latest publication by Wong and Buenfel (2006) on this topic, although no additional evidences have been provided, the assumption that the sharp increase in porosity observed in (Winslow *et al.* 1994) is related to the percolation effect cannot be falsified at least. Thus, it is still reasonable to use the experimental result in (Winslow *et al.* 1994) to validate the correctness of the developed computer program.

To compare with the result of MIP test, the aggregate gradation labelled as "Exp." in Table 1 provided in (Winslow *et al.* 1994) is used. Since the information about aggregate shape was not mentioned in the paper, different normal aspect ratios of aggregates are adopted based on Fig. 3. The ITZ percolation thresholds obtained from numerical simulation are shown in Fig. 10. It is found that with proper aspect ratios of aggregate and ITZ thickness which are both within the normal range, the ITZ percolation thresholds coincide well with that obtained from MIP test in (Winslow *et al.* 1994). Therefore, the computer program developed in this paper is validated.

4. Results and discussion

4.1 Effect of model size

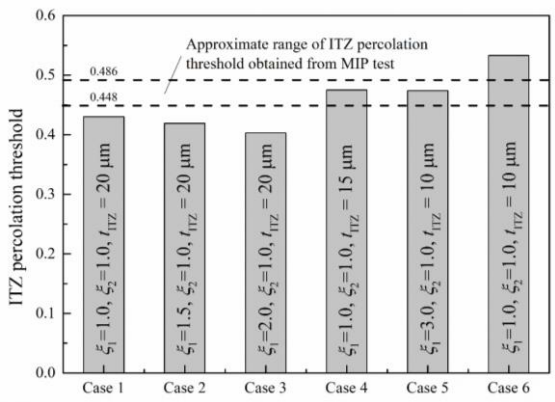

Fig. 10 A comparison between ITZ percolation thresholds from numerical simulation and MIP test by Winslow *et al.* (1994)

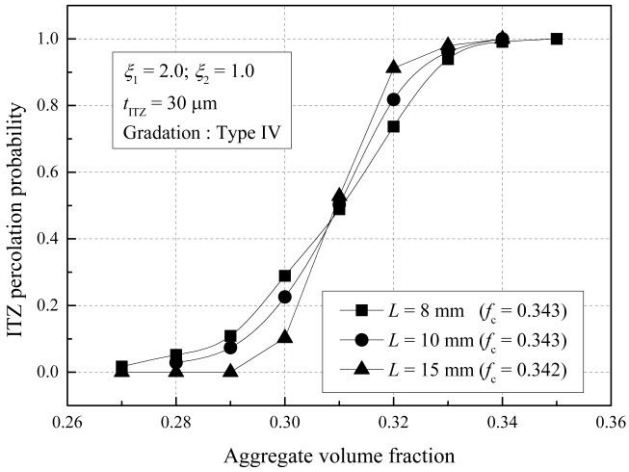

Fig. 11 Effects of REV size on percolation transition width and threshold

The number of particles in REV will dramatically increase with the size of REV, especially in a three-dimensional simulation. Thus, to speed up the simulation, a smaller REV is preferred. But it should be studied whether the size of REV has a significant effect on the ITZ percolation threshold. Thus, the parametric study on the size of REV is firstly conducted here. Three sizes of REV, i.e., $L = 8\,\text{mm},\ 10\,\text{mm}$ and $15\,\text{mm}$, are selected. The results are shown in Fig. 11. As can be seen, a larger REV will result in a smaller width of percolation transition, i.e., λ in Eq. (10), which indicates that when the size of REV reaches infinite ($L \to \infty$), a sudden jump ($\lambda \to 0$) of ITZ percolation probability will occur at the threshold. This result agrees with the qualitative analysis in (Zheng and Zhou 2007).

With three curves of ITZ percolation probability in Fig. 11, the corresponding percolation threshold can be determined by Eq. (10). The results are $f_c = 0.343, 0.343, 0.342$ for $L = 8\,\text{mm}, 10\,\text{mm}$ and $15\,\text{mm}$, respectively, which are very close to one another. Therefore, based on this parametric study, it can be concluded that the size of REV can only affect the width of percolation transition, but the threshold is almost independent of the size of REV. This result enables a free choice of the REV size used in the simulation.

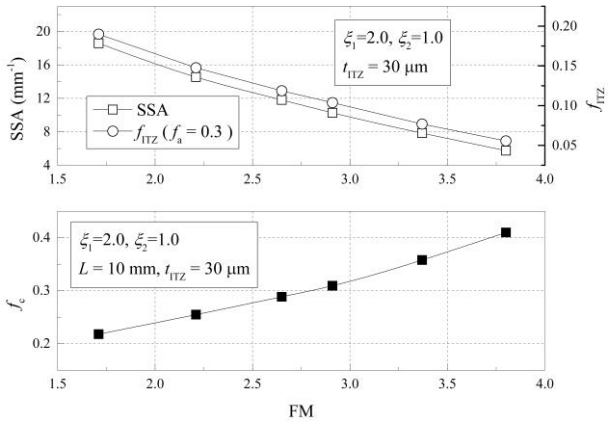

Fig. 12 Effects of aggregate fineness on ITZ percolation threshold

4.2 Effect of aggregate gradation

The results of ITZ percolation threshold for six selected aggregate gradations (Type I ~ Type VI in Table 1) are plotted in Fig. 12. As can be seen, the ITZ percolation threshold can be greatly affected by the aggregate gradation and increases with FM of gradation. The reason can be attributed to SSA of aggregates, which is also shown in Fig. 12. As expect, the gradation with a higher FM can result in a smaller SSA due to the lower percentage of small particles. Thus, the ITZ volume fraction will also increase with FM, which is calculated by the method in Section 2.1.5 and plotted in Fig. 12. With more ITZs inside the REV, a higher percolation probability and a smaller threshold can be expected.

The above result is in agreement with the findings in (Bentz *et al.* 1994) and (Zheng and Zhou 2007), which is briefly explained as follows. In (Bentz *et al.* 1994), the effect of aggregate gradation was studied by excluding the smallest particles ($< 150\,\mu$m in diameter) from the gradation. Based on Eq. (1), neglect of small particles in the gradation will result in a larger FM. It was found that a greater particle volume fraction is needed to percolate the model if small particles are removed. In (Zheng and Zhou 2007), two special gradations, i.e., Fuller's and EVF gradations, were compared with each other. Based on the expressions of these two gradations, it can be easily found that EVF has a smaller FM than the Fuller's gradation with the same maximum size of aggregate (D_{m}). For example, when $D_{\mathrm{m}} = 4.75$ mm, the FMs of the Fuller's and EVF gradations calculated by Eq. (1) are 3.426 and 3.285, respectively. It was found that EVF gradation can lead to a smaller percolation threshold compared with the Fuller's gradation. All the above findings coincide with the result in Fig. 12.

4.3 Effect of aspect ratio

Based on the distribution of aspect ratios of real aggregates in Fig. 3, $\xi_1\ (\xi_2) = 1.0, 1.5, 2.0, 2.5, 3.0$ in 25 different combinations of (ξ_1, ξ_2) are adopted to study the effect of aspect ratios of aggregates on ITZ percolation threshold. The results are shown in Table 2. As can be seen,

Table 2 ITZ percolation thresholds for different aspect ratios of aggregates

ξ_2 \ ξ_1	1.0	1.5	2.0	2.5	3.0
1.0	0.332	0.324	0.309	0.293	0.277
1.5	0.324	0.309	0.290	0.271	0.253
2.0	0.308	0.289	0.268	0.248	0.229
2.5	0.293	0.272	0.249	0.228	0.210
3.0	0.277	0.255	0.232	0.212	0.194

Note: (1) ITZ thickness is $30\,\mu$m; (2) Aggregate gradation is Type IV in Fig. 1.

Table 3 SSAs for different aspect ratios of aggregates (mm^{-1})

ξ_2 \ ξ_1	1.0	1.5	2.0	2.5	3.0
1.0	9.4346	9.6941	10.152	10.646	11.124
1.5	9.7311	10.273	10.908	11.526	12.102
2.0	10.354	11.135	11.933	12.672	13.348
2.5	11.093	12.098	13.039	13.893	14.672
3.0	11.898	13.098	14.176	15.139	16.010

Note: (1) ITZ thickness is $30\,\mu$m; (2) Aggregate gradation is Type IV in Fig. 1.

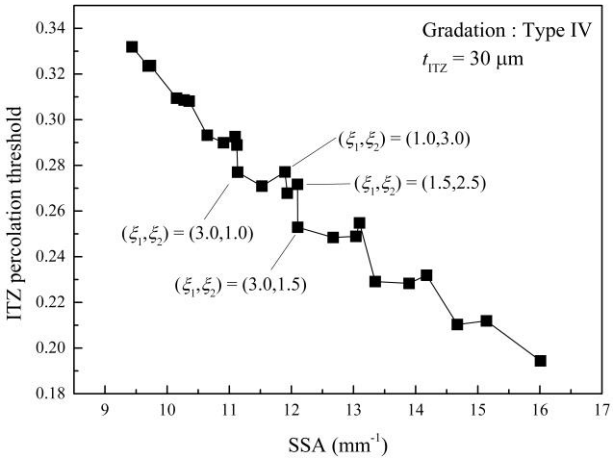

Fig. 13 Plot of ITZ percolation threshold as a function of SSA

the ITZ percolation threshold decreases with an increasing $\xi_1\ (\xi_2)$. This result is in agreement with the study in theoretical physics on "soft-core/no-shell" models (Garboczi *et al.* 1995), where spherical particles result in the largest percolation threshold.

Similar to aggregate gradation, the reason for the decreasing tendency of ITZ percolation threshold with increasing aspect ratios of aggregates can be also attributed to SSA, as SSA increases with the aspect ratios (see Table 3). However, if the ITZ percolation threshold is plotted as a function of SSA shown in Fig. 14, it is found that the threshold does not monotonously decrease with an increasing SSA. For example, SSA for $(\xi_1, \xi_2) = (1.0,3.0)$ is larger than that for $(\xi_1, \xi_2) = (3.0,1.0)$. But the thresholds in these two cases are 0.2770 and 0.2771, which are almost the same. Similar exceptions can be also found between $(\xi_1, \xi_2) = (2.5,1.5)$ and $(\xi_1, \xi_2) = (1.5,2.5)$,

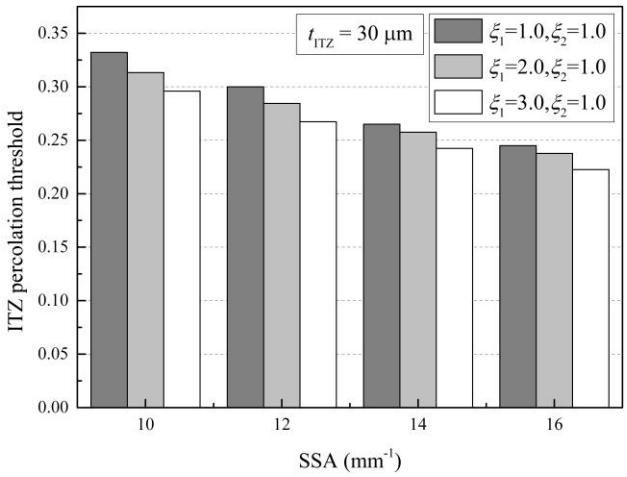

Fig. 14 Effect of major aspect ratio of aggregates on ITZ percolation threshold with same SSA

$(\xi_1, \xi_2) = (3.0,2.5)$ and $(\xi_1, \xi_2) = (2.5,3.0)$, $(\xi_1, \xi_2) = (3.0,2.0)$ and $(\xi_1, \xi_2) = (2.5,2.5)$. Furthermore, even with the same SSA, the ITZ percolation thresholds may be still different, e.g., between $(\xi_1, \xi_2) = (3.0,1.5)$ and $(\xi_1, \xi_2) = (1.5,2.5)$. All the above exceptions indicate that SSA is not the single reason for the effect of aspect ratios of aggregates on ITZ percolation threshold.

In the research on ITZ percolation in fiber-reinforced high-performance concrete (Bentz 2000), it was found that fibers can provide alternative paths to connect isolated ITZs, which can increase the percolation probability. When an ellipsoidal particle is elongated, it may have the same function as fibers due to their similar geometries. To verify this conclusion, several extra case studies are conducted here. In these cases, the major aspect ratio ξ_1 is set as 1.0~3.0, while the minor aspect ratio ξ_2 is fixed as 1.0. As ξ_1 increases, the ellipsoidal particle is more severely elongated. Since SSA changes with aspect ratios of particles (see Table 3), the gradations are slightly modified to ensure an identical SSA for different major aspect ratios to exclude the influence of SSA on ITZ percolation threshold. Four different SSAs, i.e., 10 mm^{-1}, 12 mm^{-1}, 14 mm^{-1}, 16 mm^{-1}, are investigated. Thus, totally 12 different cases are analyzed. The ITZ percolation thresholds in these cases are shown in Fig. 14. The results clearly indicate that despite the identical SAA, the ITZ percolation threshold decreases with an increasing major aspect ratio. To reveal the reasons for these results, ITZ volume fraction (f_{ITZ}) and ITZ connectivity (ϕ) are calculated and plotted in Fig. 15 and Fig. 16, respectively. As can be seen, as ξ_1 increases, f_{ITZ} slightly decreases but ϕ increases. This result indicates that when ellipsoidal particles are more severely elongated, although the ITZ volume fraction will slightly decrease, isolated ITZ clusters are more likely to be connected by ellipsoidal particles together to form a larger cluster. Thus, the increasing tendency of ϕ with ξ_1 proves the "bridging effect" from elongated ellipsoidal particles to connect isolated ITZ clusters. As a visual validation, the largest ITZ clusters in the case of $\mathrm{SSA} = 10\ \mathrm{mm}^{-1}$ are plotted in Fig. 17, which clearly illustrates the "bridging effect" from elongated particles.

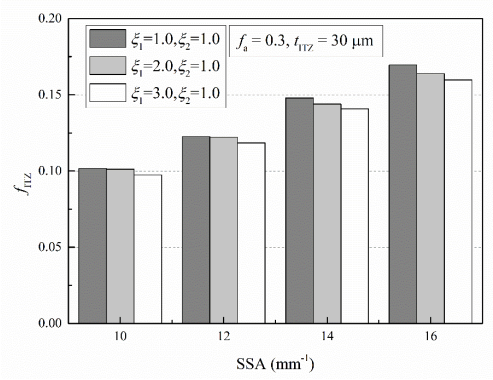

(a) f_a=0.3

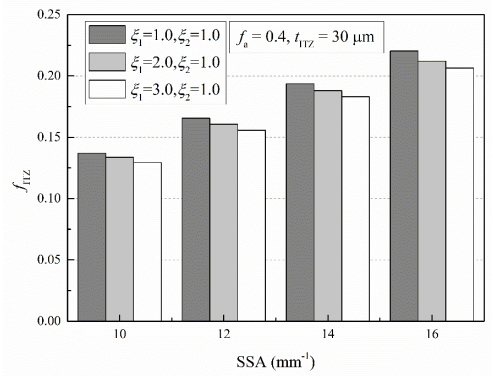

(b) f_a=0.4

Fig. 15 Effect of major aspect ratio of particles on ITZ volume fraction with same SSA

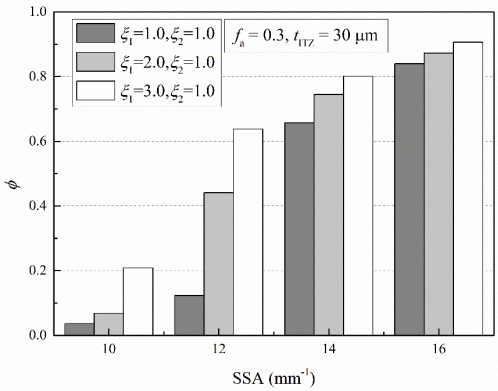

(a) f_a=0.3

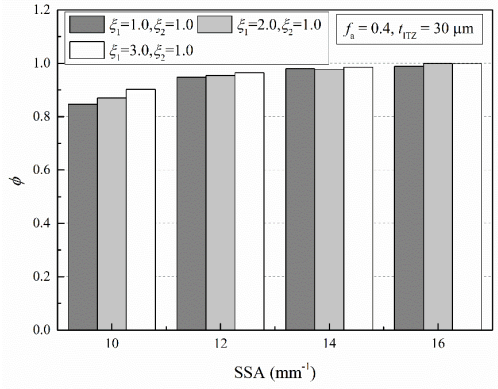

(a) f_a=0.4

Fig. 16 Effect of major aspect ratio of particles on ITZ connectivity with same SSA

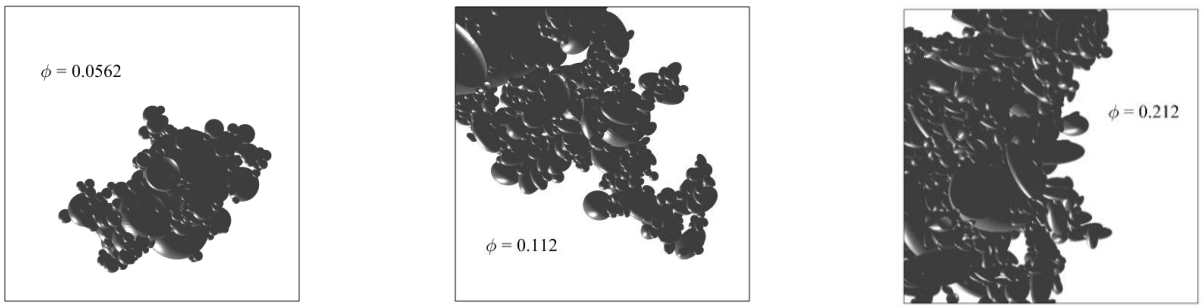

(a) $\xi_1 = 1.0$ (b) $\xi_1 = 2.0$ (c) $\xi_1 = 3.0$

Fig. 17 Identified largest ITZ clusters in meso-scale with different major aspect ratios of ellipsoidal particles

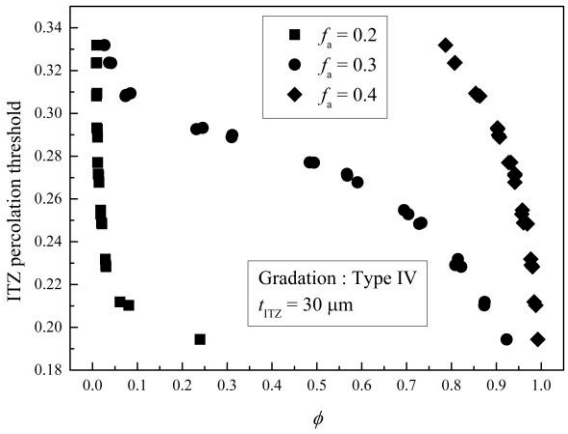

Fig. 18 Plot of ITZ percolation threshold as a function of ITZ connectivity

However, it should be mentioned that the above "bridging effect" is only of importance when f_{ITZ} is small. As shown in Fig. 16, when SSA and f_{a} increase (which can both increase f_{ITZ}), the "bridging effect" becomes less significant. The reason is obvious: as more and more ITZs are formed inside the meso-scale model, ITZ clusters will be so close to one another that no alternative paths provided by elongated particles are needed to connect them.

Based on the above analysis, it can be concluded that (1) SSA plays a major role in ITZ percolation threshold which shows a global decreasing tendency with an increasing SSA; (2) elongated ellipsoidal particles can effectively bridge isolated ITZs, thus leading to lower ITZ percolation threshold; (3) as ITZ volume fraction increases, the "bridging effect" of elongated particles will be less significant, and only has a minor effect on ITZ percolation threshold. Besides, it can be also concluded that the aspect ratios of aggregates can affect the ITZ percolation threshold in at least three aspects: (1) the SSA increases with the aspect ratio (Table 3); (2) the ITZ volume fraction slightly decreases with an increasing aspect ratio (Fig. 15); (3) the "bridging effect" caused by elongated particles increases with the aspect ratio (Fig. 16).

Based on the above conclusions, the ITZ percolation threshold is finally replotted as a function of ϕ, as shown in Fig. 18. As can be seen, the exceptions found in Fig. 13 are almost excluded. This result indicates that it is the ITZ connectivity rather than SSA or ITZ volume fraction that is essentially responsible for ITZ percolation threshold.

5. Conclusions

This paper mainly studied the ITZ percolation threshold in the mortar by a numerical simulation approach. The fine aggregate in the mortar was simplified as an ellipsoidal particle with arbitrary orientations. The effects of the gradation and aspect ratios of aggregates on ITZ percolation threshold were studied. Based on the results and discussions, the following conclusions can be made:

- The ITZ percolation threshold is mainly affected by SSA of aggregates and shows a global decreasing tendency with an increasing SSA, but SSA is not the single reason responsible for ITZ percolation threshold.
- The aspect ratios of aggregates can affect ITZ percolation threshold in at least three aspects: (1) the SSA increases with the aspect ratio; (2) the ITZ volume fraction slightly decreases with an increasing aspect ratio; (3) isolated ITZs can be more effectively bridged by ellipsoidal particles with larger aspect ratios, which can lower the ITZ percolation threshold.
- As ITZ volume fraction increases, the "bridging effect" of elongated ellipsoidal particles will be less significant, and only has a minor effect on ITZ percolation threshold.
- It is the ITZ connectivity that is essentially responsible for ITZ percolation threshold, while other factors such as SSA and ITZ volume fraction are only the superficial reasons.

Acknowledgments

The authors would like to thank the National Science Foundation of China (No. 51378383) for the financial support.

References

Bazant, Z.P., Tabbara, M.R., Kazemi, M.T. and Pijaudiercabot, G. (1990), "Random particle model for fracture of aggregate or fiber composites", *J. Eng. Mech.*, **116**(8), 1686-1705.

Bentz, D.P. (2000), "Fibers, percolation, and spalling of high-performance concrete", *ACI Mater. J.*, **97**(3), 351-359.

Bentz, D.P., Hwang, J.T.G., Hagwood, C., Garboczi, E.J., Snyder, K.A. and Scrivener, N.B.K.L. (1994), "Interfacial zone percolation in concrete: Effects of interfacial zone thickness and

aggregate shape", *Mrs Proc.*, **370**, https://doi.org/10.1557/PROC-370-437.
Delagrave, A., Bigas, J.P., Ollivier, J.P., Marchand, J. and Pigeon, M. (1997), "Influence of the interfacial zone on the chloride diffusivity of mortars", *Adv. Cement Bas. Mater.*, **5**(3-4), 86-92.
Diamond, S. (2003), "Percolation due to overlapping ITZs in laboratory mortars? A microstructural evaluation", *Cement Concrete Res*., **33**(7), 949-955.
Dijkstra, E.W. (1959), "A note on two problems in connexion with graphs", *Numerische Mathematik*, **1**(1), 269-271.
Erdogan, S.T. (2005), "Determination of aggregate shape properties using X-ray tomographic methods and the effect of shape on concrete rheology", PhD, The University of Texas at Austin, Austin, US.
Garboczi, E.J., Snyder, K.A., Douglas, J.F. and Thorpe, M.F. (1995), "Geometrical percolation threshold of overlapping ellipsoids", *Phys. Rev. E Statist. Phys. Plasmas Fluid. Relat. Interdisc. Top.*, **52**(1), 819-828.
Hafner, S., Eckardt, S., Luther, T. and Konke, C. (2006), "Mesoscale modeling of concrete: Geometry and numerics", *Comput. Struct*., **84**(7), 450-461.
King, C.Y. (2008), "Collision detection for ellipsoids and other quadrics", PhD, University of Hong Kong, Hong Kong.
Lee, K.M. and Park, J.H. (2008), "A numerical model for elastic modulus of concrete considering interfacial transition zone", *Cement Concrete Res*., **38**(3), 396-402.
Leite, J.P.B., Slowik, V. and Mihashi, H. (2004), "Computer simulation of fracture processes of concrete using mesolevel models of lattice structures", *Cement Concrete Res.*, **34**(6), 1025-1033.
Li, J. (2013), "Percolation thresholds of two-dimensional continuum systems of rectangles", *Phys. Rev. E Statist. Nonlin. Soft Mat. Phys.*, **88**(1), 012101.
Li, J. and Ô stling, M. (2016), "Precise percolation thresholds of two-dimensional random systems comprising overlapping ellipses", *Physica A Statist. Mech. Its Appl.*, **462**, 940-950.
Liao, K.Y., Chang, P.K., Peng, Y.N. and Yang, C.C. (2004), "A study on characteristics of interfacial transition zone in concrete", *Cement Concrete Res*., **34**(6), 977-989.
Lutz, M.P., Monteiro, P.J.M. and Zimmerman, R.W. (1997), "Inhomogeneous interfacial transition zone model for the bulk modulus of mortar", *Cement Concrete Res.*, **27**(7), 1113-1122.
Ollivier, J.P., Maso, J.C. and Bourdette, B. (1995), "Interfacial transition zone in concrete", *Adv. Cement Bas. Mater.*, **2**(1), 30-38.
Pan, Z., Ruan, X. and Chen, A. (2014), "Chloride diffusivity of concrete: probabilistic characteristics at meso-scale", *Comput. Concrete*, **13**(2), 187-207.
Pan, Z., Ruan, X. and Chen, A. (2015), "A 2-D numerical research on spatial variability of concrete carbonation depth at meso-scale", *Comput. Concrete*, **15**(2), 231-257.
Prokopski, G. and Halbiniak, J. (2000), "Interfacial transition zone in cementitious materials", *Cement Concrete Res.*, **30**(4), 579-583.
Qian, Z. (2012), "Multiscale modeling of fracture processes in cementitious materials", PhD, Delft University of Technology, Delft, The Netherlands.
Quintanilla, J.A. and Ziff, R.M. (2007), "Asymmetry in the percolation thresholds of fully penetrable disks with two different radii", *Phys. Rev. E Statist. Nonlin. Soft Mat. Phys.*, **76**(5), 051115.
Rintoul, M.D. and Torquato, S. (1997), "Precise determination of the critical threshold and exponents in a three-dimensional continuum percolation model", *J. Phys. A: Math. Gen*., **30**(16), L585.
Rypl, D. and Bým, T. (2012), "Geometrical modeling of concrete microstructure for the assessment of ITZ percolation", *Acta Polytechnica*, **52**(6), 1-15.
Samet, H. and Tamminen, M. (1988), "Efficient component labeling of images of arbitrary dimension represented by linear bintrees", *IEEE Tran. Pat. Anal. Mach. Intel.*, **10**(4), 579-586.
Šavija, B., Pacheco, J. and Schlangen, E. (2013), "Lattice modeling of chloride diffusion in sound and cracked concrete", *Cement Concrete Compos*., **42**, 30-40.
Scrivener, K.L. and Nemati, K.M. (1996), "The percolation of pore space in the cement paste/aggregate interfacial zone of concrete", *Cement Concrete Res*., **26**(1), 35-40.
Shane, J.D., Mason, T.O., Jennings, H.M., Garboczi, E.J. and Bentz, D.P. (2000), "Effect of the interfacial transition zone on the conductivity of Portland cement mortars", *J. Am. Ceram. Soc*., **83**(5), 1137-1144.
Wang, W.P., Wang, J.Y. and Kim, M.S. (2001), "An algebraic condition for the separation of two ellipsoids", *Comput. Aid. Geometric Des.*, **18**(6), 531-539.
Wang, Z.M., Kwan, A.K.H. and Chan, H.C. (1999), "Mesoscopic study of concrete I: generation of random aggregate structure and finite element mesh", *Comput. Struct.*, **70**(5), 533-544.
Winslow, D.N., Cohen, M.D., Bentz, D.P., Snyder, K.A. and Garboczi, E.J. (1994), "Percolation and pore structure in mortars and concrete", *Cement Concrete Res.*, **24**(1), 25-37.
Wong, H.S. and Buenfel, N.R. (2006), "Patch microstructure in cement-based materials: Fact or artefact?", *Cement Concrete Res*., **36**, 990.
Wu, K., Xu, L., Schutter, G.D., Shi, H. and Ye, G. (2015), "Influence of the interfacial transition zone and interconnection on chloride migration of portland cement mortar", *J. Adv. Concr. Technol*., **13**(3), 169-177.
Xia, W. and Thorpe, M.F. (1988), "Percolation properties of random ellipses", *Phys. Rev. A*, **38**(5), 2650-2656.
Yang, C.C. and Su, J.K. (2002), "Approximate migration coefficient of interfacial transition zone and the effect of aggregate content on the migration coefficient of mortar", *Cement Concrete Res.*, **32**(10), 1559-1565.
Yang, R., Gui, Q., Lemarchand, E., Fen-Chong, T. and Li, K. (2015), "Micromechanical modeling of transport properties of cement-based composites: Role of interfacial transition zone and air voids", *Tran. Porous Media*, **110**(3), 591-611.
Ye, G. (2005), "Percolation of capillary pores in hardening cement pastes", *Cement Concrete Res.*, **35**(1), 167-176.
Zheng, J. and Zhou, X. (2007), "Percolation of ITZs in concrete and effects of attributing factors", *J. Mater. Civil Eng.*, **19**(9), 784-790.
Zheng, X., Iglesias, W. and Palffy-Muhoray, P. (2009), "Distance of closest approach of two arbitrary hard ellipsoids", *Phys. Rev. E Stat. Nonlin. Soft Matt. Phys.*, **79**(5), 057702.
Zheng, X. and Palffy-Muhoray, P. (2007), "Distance of closest approach of two arbitrary hard ellipses in two dimensions", *Phys. Rev. E Stat. Nonlin. Soft Mat. Phys.*, **75**(6), 061709.

HK